Universal imaginary-time critical dynamics on a quantum computer

Shi-Xin Zhang[1,*] and Shuai Yin[2,†]
[1]*Tencent Quantum Laboratory, Tencent, Shenzhen, Guangdong 518057, China*
[2]*School of Physics, Sun Yat-Sen University, Guangzhou 510275, China*

(Received 29 November 2023; revised 11 April 2024; accepted 16 April 2024; published 30 April 2024)

Quantum computers promise a highly efficient approach to investigate quantum phase transitions, which describe abrupt changes between different ground states of many-body systems. At quantum critical points, the divergent correlation length and entanglement entropy render the ground state preparation difficult. In this work, we explore the imaginary-time evolution for probing the universal critical behavior as the universal information of the ground state can be extracted in the early time relaxation process. We propose a systematic and scalable scheme to probe the universal behaviors via imaginary-time critical dynamics on quantum computers and demonstrate the validness of our approach by both numerical simulation and quantum hardware experiments. With the full form of the universal scaling function in terms of imaginary time, system size, and circuit depth, we successfully probe the universality by scaling analysis of the critical dynamics at an early time and with shallower quantum circuit depth. Equipped with quantum error mitigation, we also confirm the expected scaling behavior from experimental results on a superconducting quantum processor which stands as the first experimental demonstration of universal imaginary-time quantum critical dynamics.

DOI: 10.1103/PhysRevB.109.134309

I. INTRODUCTION

Quantum computing has been of great academic and industrial interest since Richard Feynman's original vision of using quantum systems to simulate nature. Recently, various experimental platforms of noisy intermediate-scale quantum (NISQ) [1] devices have been developed, with the long-term vision for solving practical problems that a classical computer cannot address efficiently [2,3]. Moreover, quantum algorithms for quantum simulation of ground state, excited state, and dynamical properties have expanded in recent years [4–7]. Various quantum error mitigation (QEM) techniques [8–14] have also been developed to alleviate the effect of quantum noise on NISQ devices and yield reliable experimental results. The rapid development of quantum hardware, quantum algorithms, and quantum software provides far-reaching platforms to investigate various exotic quantum phases.

As the watershed of different ground states, the critical points hold universal scaling behaviors, attracting extensive investigations as one of the cornerstones of modern physics [15]. Critical exponents are crucial to determine the universality class of the corresponding critical points, which is the most important aspect of a quantum phase transition and is the key to developing correct theoretical understanding for these transitions. The routine method to explore the critical properties in ground states is to identify ground states first and then reveal the scaling properties of physical quantities defined on ground states. However, for critical systems, difficulties are encountered in obtaining the ground state with quantum computers. Quantum circuits should be carefully chosen to take into account the divergent entanglement which in general requires a divergent depth of quantum circuits to faithfully capture. In addition, the typical time scale to arrive at the ground state in imaginary-time evolution is proportional to N^z in which N is the system size and z is the dynamic exponent. Therefore, for large systems, it takes an extremely long time to obtain the ground state accurately via imaginary time evolution.

In this work, we show that these disadvantages in probing quantum critical properties can be transformed into advantages by exploring universal scaling behaviors in the imaginary-time critical dynamics on quantum computers. Firstly, we identify that critical exponents appearing in the short-time dynamical scaling are the same as the static ones in the ground state. We can circumvent the need to get ground state based on this connection. Secondly, starting from a product state, both the correlation length and entanglement entropy are relatively small in the short-time stage. Therefore we can infer the late-time (ground state) universal behavior via the short-time scaling at the early time. Finally, even if the shallow variational circuits fail to faithfully reflect the imaginary-time dynamics, we can still extract the correct universal scaling based on finite-depth scaling. In sum, the universal properties of the critical point can be detected in an efficient and scalable way with short imaginary time evolved and shallow variational circuit required.

By using the powerful toolboxes for quantum simulation on NISQ devices, including the variational quantum eigensolver (VQE) [7,16–22], variational quantum dynamics simulation [23–27], and quantum error mitigation, we reveal the scaling form of imaginary-time critical dynamics on quan-

*shixinzhang@tencent.com
†yinsh6@mail.sysu.edu.cn

tum computers in the one-dimensional quantum Ising model. Our results not only experimentally demonstrate the universal imaginary-time critical dynamics for the first time, but also pave the way for future studies on novel critical systems via imaginary-time dynamics on NISQ computers.

II. IMAGINARY-TIME CRITICAL DYNAMICS

There are two types of dynamical critical behaviors often discussed in the literature: one is the real-time annealing dynamics characterized by the famous Kibble-Zurek mechanism and its generalizations [28–32], and the other one is the short-time critical scaling in the imaginary-time quench process. Note that the real-time unitary relaxation dynamics after a sudden quench usually cannot reflect the scaling properties of the quantum critical point at the ground state [30,31]. The Kibble-Zurek dynamical critical scaling has been extensively studied in various settings and shows its power in different quantum platforms, such as D-Wave annealer [33], Rydberg arrays [34], ultracold atoms [35,36] and trapped ions [37], to assess the quality of the preparation of the putative ground states. On the contrary, the imaginary-time short-time dynamical critical behavior has never been explored in experiments.

The imaginary-time evolution of a quantum system described by a Hamiltonian H for a quantum state $|\psi(t)\rangle$ has a formal solution as a nonunitary evolution $e^{-\tau H}$ on the initial state $|\psi(0)\rangle$:

$$|\psi(\tau)\rangle = \frac{1}{Z}\exp(-H\tau)|\psi(0)\rangle, \tag{1}$$

where $Z = \langle\psi(0)|\exp(-2H\tau)|\psi(0)\rangle$ is the normalization factor.

When H is near its critical point, the universal scaling behaviors emerge in the imaginary-time relaxation process [38–42]. From a product initial state with an initial order parameter M_0, the general scaling transformation of a physical quantity P follows [38]

$$P(\tau, g, M_0, N) = b^{\phi}P[b^{-z}\tau, b^{1/\nu}g, U(b, M_0), b^{-1}N], \tag{2}$$

in which b is the rescaling factor, g is the distance in Hamiltonian parameter deviating from the critical point, ϕ is the scaling dimension of P, and $U(b, M_0)$ is a characteristic function [43]. For $M_0 = 1$, we have the fixed point $U(b, M_0) = 1$.

This scaling function (2) was first proposed in classical critical dynamics [43–47] and then generalized to quantum imaginary-time critical dynamics owing to the dissipative nature of evolution in both cases [38,39]. The critical exponents in Eq. (2) are the same as the equilibrium ones since they are connected via $\tau \to \infty$ limit, when Eq. (2) should recover the equilibrium scaling for ground states.

By extending to the finite circuit depth case [48,49], where the static or dynamical states are prepared by a finite-depth variational quantum circuit, we have

$$P(\tau, g, M_0, N, D) = b^{\phi}P[b^{-z}\tau, b^{1/\nu}g, \times U(b, M_0), b^{-1}N, b^{-\alpha}D], \tag{3}$$

where D is the circuit depth and α is its scaling dimension. Previous work has revealed such finite-depth scaling for ground state preparation on quantum computers and our work explores the finite-depth scaling in dynamics for the first time.

From a completely ordered initial state, for $P = M^k$, the kth moment of the order parameter with $\phi = -k\beta/\nu$, by choosing $b = N$, one obtains the scaling form of M^k at $g = 0$ as

$$M^k(\tau, N, D) = N^{-k\beta/\nu}f_M(\tau N^{-z}) \tag{4}$$

and

$$M^k(\tau, N, D) = N^{-k\beta/\nu}f_M(\tau N^{-z}, DN^{-\alpha}), \tag{5}$$

with finite-depth consideration.

From a disordered initial state with the local order parameter distributed randomly and $M_0 = 0$, an imaginary-time correlator is defined as $A \equiv \overline{(\sum_{i=1}^{N} M_i^s(0)M_i^s(\tau))_s}$, where the correlator is average over different initial spin configuration s as well as qubit i. This correlator satisfies the dynamic scaling form as

$$A = N^{-d+\theta z}f_A(\tau N^{-z}), \tag{6}$$

in which θ is the critical initial slip exponent, unique to the dynamical behavior.

III. VARIATIONAL IMAGINARY-TIME DYNAMICS SIMULATION

There are two main proposals to enable the simulation of nonunitary imaginary-time dynamics on quantum computers. The Trotterization-based approach [50], implements the unitary approximation for each small Trotterized imaginary time step progressively which requires a large circuit depth: exponential with respect to the correlation length and linear with respect to the evolved time. This method is thus not ready for NISQ devices.

The ansatz-based approach, on the other hand, has a predefined variational circuit ansatz U. Given a set of variational circuit parameters $\vec{\theta}$, the output quantum state from the ansatz $|\phi(\vec{\theta}(\tau))\rangle = U(\vec{\theta})|0\rangle$ is taken as the imaginary-time evolved quantum state. For imaginary time τ, by determining the optimal parameters $\vec{\theta}(\tau)$, we can obtain the quantum state $|\phi(\tau)\rangle$ and thus the dynamics. Therefore the problem of dynamics simulation is reduced to determining the variational circuit parameters $\vec{\theta}(\tau)$ at different τ [24,25,51,52].

The caveat of the ansatz-based approach is that the expressive power of the circuit ansatz limits the approximation accuracy for the dynamics. However, we will utilize this aspect as finite circuit depth scaling which turns out to be helpful instead of harmful in identifying universal properties.

The time evolution dynamics for the circuit parameters under the Hamiltonian H can be derived from McLachlan's variational principle [25]:

$$\sum_j G^R_{i,j}\dot{\theta}_j = -C^R_i, \tag{7}$$

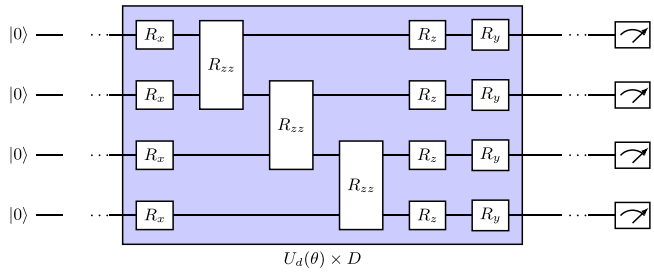

FIG. 1. The variational circuit ansatz for simulating imaginary time evolved state under 1D TFIM Hamiltonian.

where θ is the parameters in the variational circuit and $\cdot^R$ is for taking the real part. The matrix of G and the vector of C are given by

$$G_{i,j} = \frac{\partial \langle \phi(\vec{\theta}(\tau))|}{\partial \theta_i} \frac{\partial |\phi(\vec{\theta}(\tau))\rangle}{\partial \theta_j}, \tag{8}$$

$$C_i = \frac{\partial \langle \phi(\vec{\theta}(\tau))|}{\partial \theta_i} H |\phi(\vec{\theta}(\tau))\rangle, \tag{9}$$

respectively. The matrix elements can all be obtained from the real quantum hardware [25]. The dynamics in Eq. (7) can be solved as a set of ordinary differential equations using Runge-Kutta method (see Appendix A).

Throughout the work, we use the one-dimensional (1D) ferromagnetic coupled transverse field Ising model (TFIM) with open boundary conditions as the testbed, whose Hamiltonian is

$$H = \sum_{i=1}^{N} hX_i - \sum_{i=1}^{N-1} Z_i Z_{i+1}, \tag{10}$$

The quantum critical point is at $h = \pm 1$, and the critical exponents are $\beta = 1/8$, $\nu = 1$, $z = 1$ and $\theta \approx 0.373$ [38]. The local order parameter for this quantum spin model is defined as $M = \sum_i^N \langle Z_i \rangle$ with $M_0 = M(\tau = 0)$ the order parameter for the initial states.

The variational circuit ansatz is given as the hardware efficient ansatz:

$$U(\theta) = \prod_{d=1}^{D} U_d(\theta_d), \tag{11}$$

where for each circuit block we have (two-qubit gates are in ladder layout) as Fig. 1:

$$U_d(\theta_d) = \prod_{i=1}^{N} e^{-i\theta_{id4} Y_i} e^{-i\theta_{id3} Z_i} \prod_{i=1}^{N-1} e^{-i\theta_{id2} Z_i Z_{i+1}} \prod_{i=1}^{N} e^{-i\theta_{id1} X_i}. \tag{12}$$

The ansatz also shares similarities to the so-called Hamiltonian variational ansatz [53] which includes gates corresponding to the Hamiltonian terms such as $e^{i\theta X}$ and $e^{i\theta ZZ}$ in the quantum Ising model case.

IV. NUMERICAL RESULTS

We carried out the numerical simulation using quantum software TENSORCIRCUIT [54]. For detailed settings and hyperparameters, see Appendixes B, C, and D). At first, we focus on the case for sufficiently large D such that the finite depth effects can be safely ignored. For the circuit ansatz and the system size N under investigation, we observe that the number of circuit blocks $D > N/2$ is sufficient to accurately represent the imaginary dynamics with relatively small errors (see Appendix E).

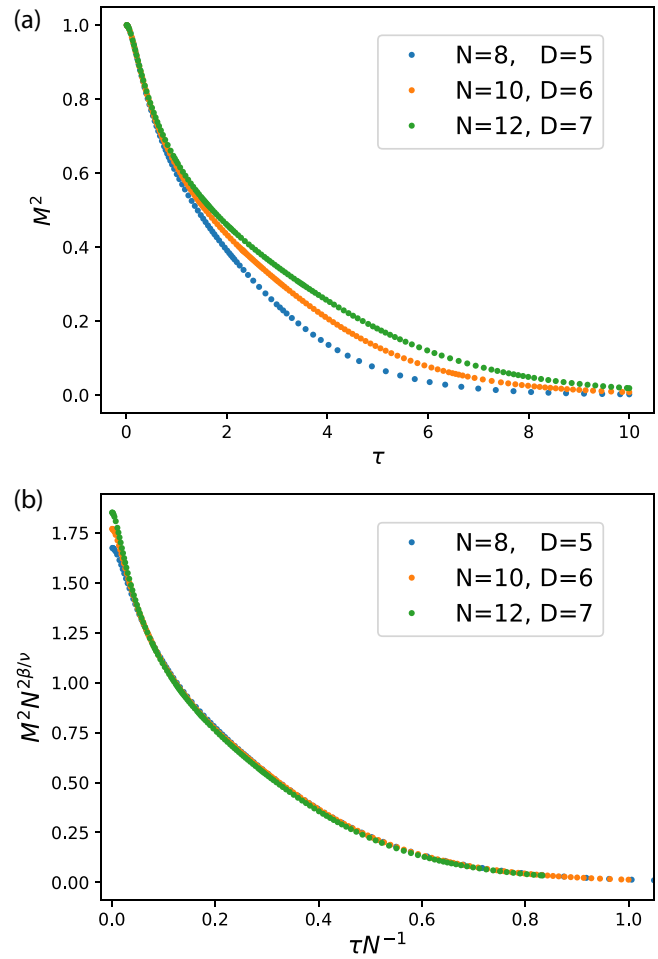

FIG. 2. (a) Unscaled and (b) finite-size scaled data for variational imaginary-time dynamics using variational circuits of different size and depth $D = N/2 + 1$ starting from $M_0 = 1$ initial state. The scaling regime begins when $\tau \gtrsim 0.1N$. The critical exponent is estimated as $\beta/\nu \approx 0.124 \pm 0.03$ for the best collapse of rescaled data.

We study the imaginary-time critical dynamics starting from $|\uparrow^n\rangle$ with $M_0 = 1$ in the imaginary time range $0 \leqslant \tau \leqslant 10$. By rescaling the order parameter measured from variational circuit with $D \geqslant N/2$ as $M^2 N^{2\beta/\nu}$ and imaginary time τ as τ/N, we find that the rescaled curves collapse well as shown in Fig. 2(b), verifying Eq. (4). The critical exponent is estimated as $\beta/\nu \approx 0.124 \pm 0.03$ for the best data collapse, consistent with the exact value $\beta/\nu = 0.125$. From Fig. 2, we identify that scaling behaviors have already emerged at the short-time stage when the system is far away from the ground state, demonstrating that the critical properties can be detected in the short-time relaxation stage using quantum computers.

Apart from the equilibrium critical exponents, the critical initial slip exponent θ unique to the dynamics can also be detected in the imaginary-time relaxation process (see Appendix F).

Next, we explore and utilize the finite-depth effects in imaginary-time critical dynamics. It was shown that circuit depth D enters the scaling form as finite-depth scaling [48,49] - a unique feature for simulation on quantum computers. In the imaginary-time dynamics, we verify Eq. (5) directly and estimate the value of circuit depth exponent α as well as the critical exponent β/ν. We select several groups of data points with sharing τN^{-1}, i.e., fixing the first variable of Eq. (5). The data points are from circuits of depth D from 2 to $N/2+2$ with system size $N = 8,\ 10,\ 12$. By rescaling D and M as $DN^{-\alpha}$ and $MN^{\beta/\nu z}$, we identify that for $\alpha \approx 1.19 \pm 0.03$ and $\beta/\nu \approx 0.126 \pm 0.04$, as shown in Fig. 3, confirming the scaling behavior Eq. (5) (see Appendix G for details on the procedure for data collapse). The extracted finite-depth exponent α is consistent with the exponent reported in [49] for translational invariant infinite-size circuits on the same model. Furthermore, the value of α is further verified directly via the scaling form of the ground state by VQE simulation in Appendix H, where different circuit ansatzes give the same finite-depth exponent, demonstrating the universality of finite-depth scaling.

Due to finite-depth and short-time scaling, to extract critical exponents, the variational circuit required does not even need to faithfully reflect the critical dynamics. We can obtain qualitatively correct estimations on these critical exponents from data at very early times and with very shallow circuits as detailed in Appendix I.

V. QUANTUM HARDWARE EXPERIMENTS

We also carried out experiments on a 20-qubit superconducting processor [55], and the variational imaginary-time dynamics results for $N = 6,\ 7,\ 8$ as well as data collapse of them according to short-time critical dynamics are shown in Fig. 4. The quantum hardware specs are listed in Appendix J while additional experimental results comparison is shown in Appendix K. In experiments, we directly load the numerically exact circuit parameters for different time τ and evaluate the order parameter $M = \sum_i^N \langle Z_i \rangle$.

To accurately evaluate M from quantum computers, several quantum error mitigation approaches [8] are utilized in our experiment. We apply readout error mitigation on observable expectation [56] and extended Clifford data regression [10,11] to mitigate both readout error and quantum gate error, respectively. The detailed error mitigation procedure is introduced in Appendix L. The mitigated results with only the former method are labeled as *raw* in Fig. 4 while the mitigated results with both mitigation methods are labeled as *mit* in Fig. 4. The accuracy for *raw* results is not sufficient to observe universal imaginary-time dynamics due to the large quantum noise present on the quantum chip while the accuracy for *mit* results can be helpful in identifying the finite-size short-time critical scaling as shown in Fig. 4(d). The result is the first experimental demonstration of short-time critical dynamics.

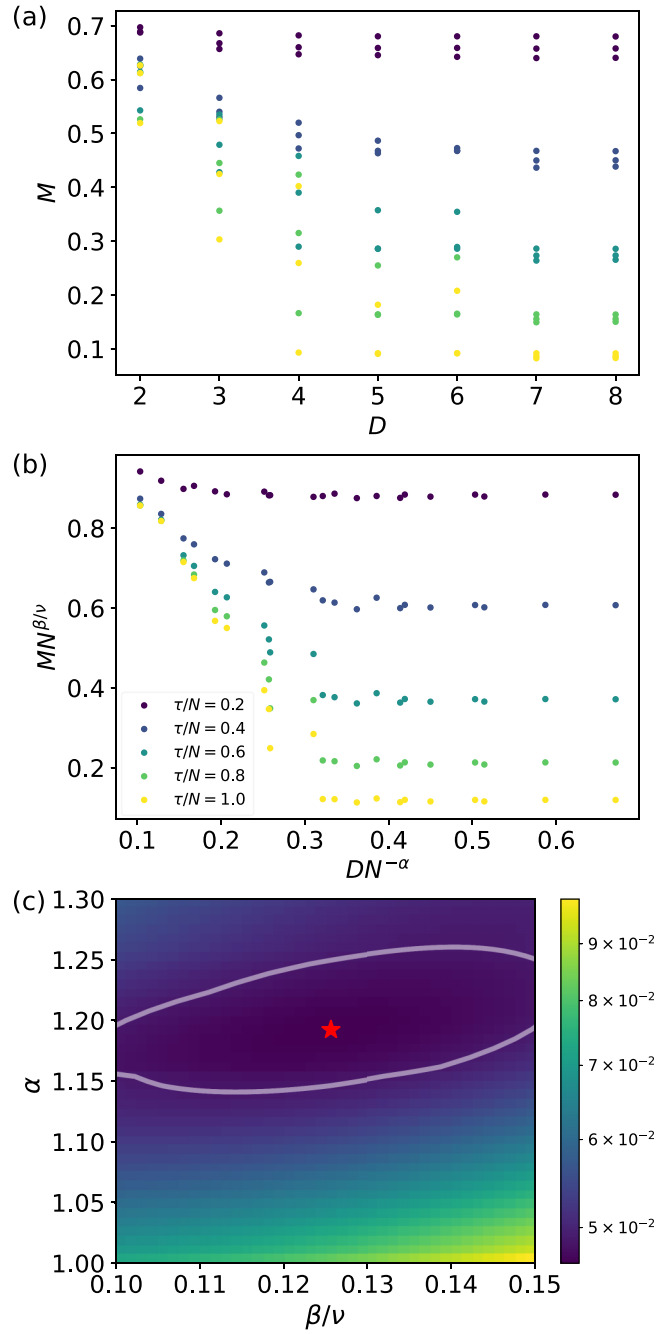

FIG. 3. Imaginary-time dynamics data with several τ/N and different D (a) unscaled and (b) rescaled according to the short-time finite-depth scaling. Points in the same color should fall into the same curve with the rescaled axis according to the finite depth exponent. (c) The data collapse quality for different guesses of finite-depth exponent α and critical exponent β/ν. The best fit is estimated at $\alpha = 1.19 \pm 0.03$ and $\beta/\nu = 0.126 \pm 0.04$. The grey contour indicates the region where the data collapse quality is no worse than 5% compared to the optimal estimation.

VI. DISCUSSIONS

Identifying quantum critical dynamics in imaginary time on quantum computers is not only of demonstration value but also paves a new way to investigate universal behaviors of critical quantum systems. Previously, to study the universal behavior of a critical system via variational quantum algorithms, one utilizes VQE to approximate the ground state at and near criticality to obtain the order parameter scaling behaviors. However, the ground state of a critical quantum

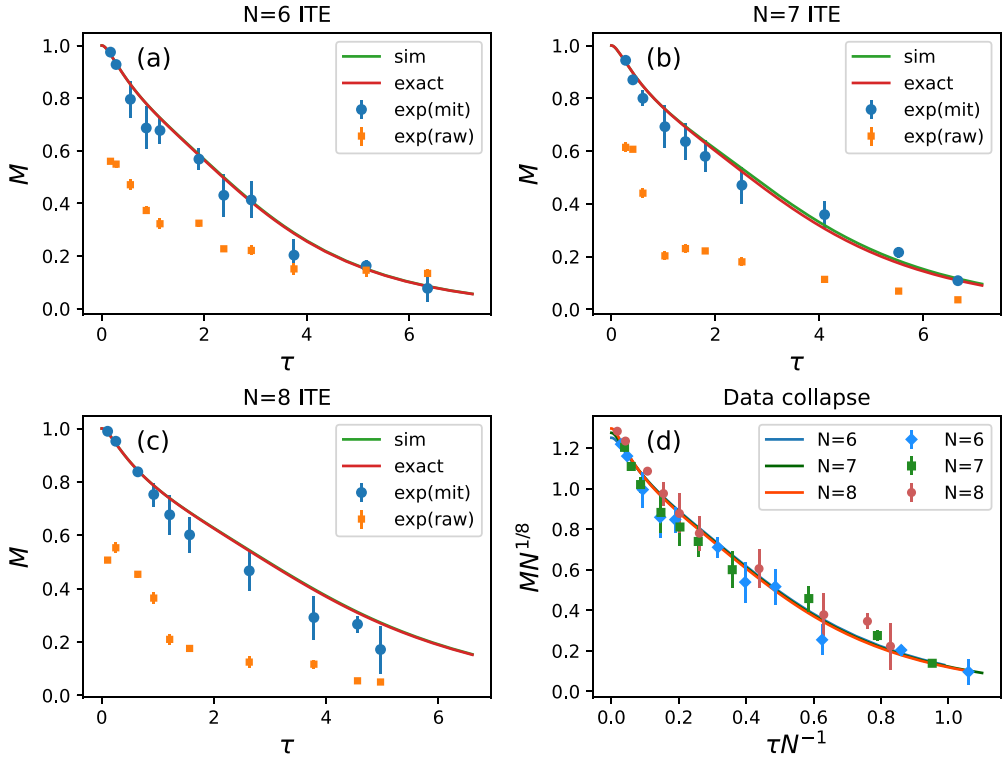

FIG. 4. Experimental demonstration of the universal short-time quantum critical dynamics in imaginary time: the experimental data are collected from a programmable superconducting quantum processor. In (a), (b), and (c), we show experimental results with only readout error mitigation (raw) and with extended Clifford data regression mitigation (mit) for $N = 6,\ 7,\ 8$ qubits and $D = 3,\ 3,\ 4$ variational circuit blocks, respectively. The exact results (exact) and numerical simulation results (sim) for the variational imaginary time evolution algorithm are also shown as lines for guidance. In (d), we apply data collapse on error mitigated data points to extract universal critical scaling from short-time dynamics, and the results coincide well with the theory prediction.

system has a logarithmic law entanglement entropy $S \sim \ln N$, which requires a large circuit depth to fully capture. Instead, via universal quantum imaginary-time dynamics, the scaling behavior with the same sets of critical exponents can be revealed at very early time $\tau \ll N$ with shallow circuits having larger approximation errors. At that early stage, the half-chain entanglement scaling is given by the universal behavior $S \sim \ln \tau$ starting from zero, much less than the ground state case. In addition, the depth of the variational circuit can be further reduced as reaching entanglement of $S \sim \ln \tau$ is also not necessary thanks to the finite-depth scaling. Therefore, via the lens of universal imaginary-time critical dynamics, much less quantum computational resources are sufficient to investigate critical phenomena compared to ground state simulation. Moreover, these benefits and potential quantum advantages of the imaginary-time critical dynamics toolbox can also manifest themselves in higher dimensional critical systems where conventional classical methods fail.

It is also an interesting future direction to study the scaling behavior of variational imaginary time dynamics with intrinsically distinct circuit architectures such as multiscale entanglement renormalization ansatz [57–60] or with dynamical circuit structures via adaptive scheme [61] or architecture search scheme [62–65].

In sum, we present the first experimental demonstration of imaginary-time short-time critical dynamics. Based on such critical behaviors, we propose a new scalable and NISQ-friendly approach with a unified scaling form of circuit depth, evolved time, and system size to study quantum critical behavior on quantum computers efficiently.

ACKNOWLEDGMENTS

We would like to acknowledge the helpful discussion with Hong Yao. S.-.X.Z. would like to acknowledge the discussion and collaboration on a related error mitigation project with Yu-Qin Chen. S.Y. is supported by the National Natural Science Foundation of China, Grants No. 12075324, No. 12222515 and the Science and Technology Projects in Guangdong Province, Grant No. 2021QN02X561.

APPENDIX A: IMAGINARY TIME DYNAMICS ON QUANTUM COMPUTERS

There are two main proposals to enable the simulation of nonunitary imaginary-time dynamics on quantum computers. The Trotterization based approach, often called QITE [50], implements the unitary approximation for each small Trotterized imaginary time step on the circuit progressively which requires an exponential large circuit depth with respect to the correlation length and a linear large circuit depth with respect to the evolved time. Therefore this method doesn't scale well with system size and is not ready for NISQ devices even with only several qubits.

The ansatz-based form, on the other hand, has a predefined variational circuit ansatz U. Given a set of variational circuit parameters $\vec{\theta}$, the output quantum state from the ansatz $|\phi(\vec{\theta}(\tau))\rangle = U(\vec{\theta})|0\rangle$ is taken as the variational quantum state under the imaginary time dynamics. For imaginary time τ, by determining the optimal parameters $\vec{\theta}(\tau)$, we can obtain the quantum state $|\phi(\tau)\rangle$ and thus the relevant observables from the state. Therefore the problem of simulating the dynamics of the quantum state is reduced to determining the dynamics of the circuit parameters $\vec{\theta}(\tau)$.

There are two approaches to determine the circuit parameter dynamics. The first approach [24,25] utilizes the philosophy of McLachlan's variational principle [66]. The circuit parameters are evolved by an ordinary differential equation whose coefficients can be obtained given the knowledge of the variational quantum state $|\phi(\vec{\theta})\rangle$.

The second approach of the ansatz-based family, called p-VQD [51,52], determines $\vec{\theta}(\tau)$ by constructing a variational optimization problem in each imaginary time step $d\tau$. In this approach, we tune $\vec{\theta}(\tau)$ to maximize the objective: $\langle\phi(\vec{\theta}(\tau))|e^{-\tau H}|\phi(\vec{\theta}(\tau - d\tau))\rangle$. The small step of nonunitary evolution in between is easy to implement by embedding the nonunitary into a Hilbert space with an extra qubit and applying only one bit of post-selection [67]. In the limit of $d\tau \to 0$, p-VQD recovers the result of McLachlan's variational principle, assuming the optimization problem is perfectly solved in each step. So the two approaches give identical circuit parameter dynamics trajectory in the ideal case. Numerically, p-VQD might be less stable than McLachlan's variational principle, as the former heavily relies on variational optimization with potential local minimum issue while the latter directly gives the exact formula for the circuit parameter dynamics and avoids explicit optimization procedures. The optimization requires gradient descent where circuit parameter gradients are obtained via parameter shift scheme in experiments or more efficiently simulated classically via automatic differentiation.

The time evolution dynamics for the circuit parameters under the Hamiltonian H can be derived from McLachlan's variational principle [25]:

$$\sum_j G^R_{i,j}\dot{\theta}_j = -C^R_i, \tag{A1}$$

where θ is the parameters in the variational circuit and $\cdot^R$ is for taking the real part. The matrix of G and the vector of C are given by

$$G_{i,j} = \frac{\partial\langle\phi(\vec{\theta}(\tau))|}{\partial\theta_i}\frac{\partial|\phi(\vec{\theta}(\tau))\rangle}{\partial\theta_j}, \tag{A2}$$

$$C_i = \frac{\partial\langle\phi(\vec{\theta}(\tau))|}{\partial\theta_i}H|\phi(\vec{\theta}(\tau))\rangle, \tag{A3}$$

respectively. The matrix elements can all be obtained from the real quantum hardware [25]. In the numerical simulation, the matrix G and the vector C can be much more efficiently obtained via unique features including vectorized parallel processing and automatic differentiation for Jacobians in TENSORCIRCUIT [54].

It is worth noting that the assumption for Eq. (A2) is the variational state is up to a fixed global phase. The more general form of the variational dynamics gives

$$G_{ij} = \frac{\partial\langle\phi(\vec{\theta}(\tau))|}{\partial\theta_i}\frac{\partial|\phi(\vec{\theta}(\tau))\rangle}{\partial\theta_j} - \frac{\partial\langle\phi(\vec{\theta}(\tau))|}{\partial\theta_i}|\phi(\vec{\theta}(\tau))\rangle\langle\phi(\vec{\theta}(\tau))\frac{\partial|\phi(\vec{\theta}(\tau))\rangle}{\partial\theta_j}. \tag{A4}$$

In terms of the one-dimensional quantum Ising model used in our work, the two forms of G matrix yield quantitatively similar results.

We can solve the dynamics Eq. (A1) by regarding it as a set of ordinary differential equations with initial vector value θ_0. We use the ODE solver with Runge-Kutta method provided by SCIPY [68] (scipy.integrate.odeint) to solve the dynamics governed by Eq. (A1). This ODE approach is more reliable and efficient compared to simple update given by discrete time steps ϵ as $\vec{\theta}(\tau + \epsilon) = \vec{\theta}(\tau) - \epsilon G^{-R}C^R$.

APPENDIX B: INITIAL PARAMETERS IN THE VARIATIONAL DYNAMICS SIMULATION

In this section, we show that with the circuit ansatz in the main text and TFIM Hamiltonian, the variational dynamics simulation is constrained and fails to reproduce the correct quantum imaginary-time dynamics if the initial circuit parameters are all strictly zero at the beginning (starting from perfect $|\uparrow^N\rangle$ state).

Recall the time evolution dynamics for the circuit parameters under the Hamiltonian H based on McLachlan's variational principle in Eq. (A1). The matrix of G and the vector of C are given as in Eqs. (A2) and (A3), respectively.

We consider the general case when only circuit parameters of Ry gates are nonzero. If we can show that in this case C are zero everywhere except at the Ry gates position, we know that the circuit parameter can only evolve nontrivially on Ry parameter subspace which fails to capture the imaginary-time dynamics variationally. This failure is not due to the low expressive power of the ansatz as the ansatz can correctly express the evolved state given appropriate circuit parameters. Instead, the failure is from the interplay between the initial parameters and the Hamiltonian which we call the phenomena variational dynamical constraint. Since we study the system evolved from $|0^N\rangle$ ($M = 1$) initial state, all initial circuit parameters are zero in the given ansatz and fall into the category of variational dynamical constraint failure. Therefore, to correctly characterize the dynamics in the numerical simulation, we perturb the initial circuit parameter from zeros at the beginning, where the perturbation is small enough to not affect the correctness of the dynamics and large enough to avoid the variational dynamical constraint failure.

Suppose we evaluate the ith element of C vector and the ith parameter is binding to a Pauli operator $P = \prod_{i\in S} P_i$ as a rotation gate $e^{-i\theta_i P}$ which is not Y (C elements corresponding to Ry gate can have nonzero amplitude),

we have

$$C_i = \mathrm{Re}\langle 0| \prod_{i=0}^{N-1} e^{i(\theta_i+\theta_i')Y_i} H \prod_{i=0}^{N-1} e^{-i\theta_i' Y_i} \cdots (-iP) \prod_{i=0}^{N-1} e^{-i\theta_i Y_i} |0\rangle$$
$$\propto \mathrm{Im}\langle\phi|H \prod_{i\in S} (P_i e^{-2i\theta_i' Y_i})|\phi\rangle, \tag{B1}$$

where we have $|\phi\rangle = e^{-i(\theta_i+\theta_i')Y_i}|0\rangle$, $\langle\phi|Y_i|\phi\rangle = 0$. We can easily check that C_i in Eq. (B1) is zero for $P = X_i$, $P = Z_i$ and $P = Z_i Z_{i+1}$ which correspond gate types in the ansatz we use. Therefore the dynamics can only evolve in the subspace of Ry gate freedom if the initial condition is strictly zero for all other gate parameters. And from the derivation, we clearly see that the simulation failure is not from the symmetry argument, instead, it is determined by the special interplay of several factors: the form of the ansatz, the form of the Hamiltonian, and the initial parameter choice.

APPENDIX C: QUANTUM SOFTWARE FRAMEWORK

All the high performance numerical simulations, as well as the quantum hardware experiments in this work, are conducted with TENSORCIRCUIT [54]: an open-source, high-performance, full-featured quantum software framework for the NISQ era. The long-term vision of TENSORCIRCUIT is to unify the infrastructures and paradigms of quantum programming by providing unified backends, unified devices, unified providers, unified resources, unified interfaces, unified engines, unified representations, and unified pipelines. The software can simulate the quantum circuit with advanced tensor network contraction engine and supports modern machine learning engineering paradigms: automatic differentiation, vectorized parallelism, just-in-time compilation, and GPU compatibility. The software also supports CPU/GPU/QPU hybrid deployment with an integrated quantum error mitigation toolbox for quantum hardware SDK. TENSORCIRCUIT has been designed to interface with various quantum cloud providers, which allows users to seamlessly access and utilize different quantum computing platforms through the unified interface.

APPENDIX D: HYPERPARAMETERS IN NUMERICAL SIMULATION

For variational quantum dynamics simulation, all zero initial parameters are perturbed with a Gaussian distribution with center zero and standard deviation 0.002 to avoid the constraint on Hilbert space of only Ry rotation as discussed before. The quantum Fisher information matrix in the parameter dynamics equation can have very bad condition numbers, so we add $10^{-7}I$ to the matrix before getting its inverse to increase the numerical stability. We use RK45 ODE solver in scipy (scipy.integrate.odeint) with default settings and a relative tolerance rtol 10^{-4}.

For variational quantum ground state simulation, we run the gradient descent 10000 steps to ensure the convergence with the Adam optimizer. We design a learning rate schedule that exponentially decays from 0.02 with a decay step 2000 for a 60% drop. Namely the learning rate at iteration step i is controlled by $\epsilon(i) = 0.02 \times 0.6^{i/2000}$. The hyperparameter of the optimizer is tuned as such for better convergence speed and accuracy. We run 64 sets of different random initialization from a Gaussian distribution center at zero with a standard deviation 0.1, among these converged results, the best one is reported as the final converged value to avoid local minimum.

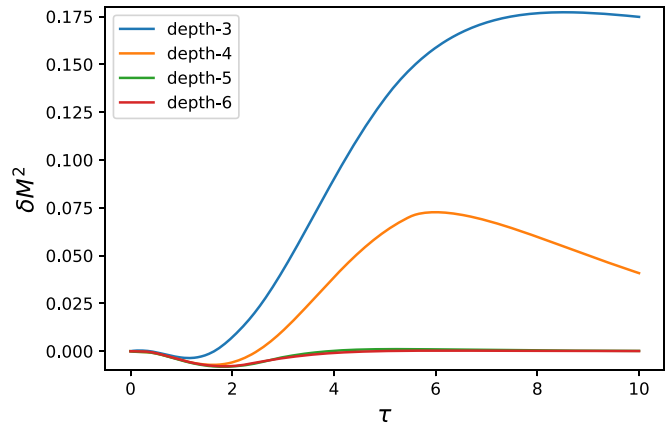

FIG. 5. The absolute error in terms of M^2 for $N = 10$ system variational quantum dynamics simulation of different circuit ansatz depth quenched from $|\uparrow^n\rangle$. The error is relatively small and saturates when the circuit depth exceeds half of the system size N.

APPENDIX E: VARIATIONAL DYNAMICS ERROR WITH DIFFERENT CIRCUIT DEPTHS D

Figure 5 shows the variational dynamics simulation error in terms of δM^2 compared to the analytic exact imaginary-time dynamics results obtained by exact diagonalization. The system Hamiltonian is 10-qubit 1D TFIM with open boundary conditions. We conclude that the approximation is good enough for the circuit depth $D > N/2$ at least in the system size range that we explored in this work.

APPENDIX F: SCALING RESULTS OF IMAGINARY-TIME CORRELATOR

We study imaginary-time-correlator A from a set of disordered initial state $M_0 = 0$ via the variational quantum imaginary-time dynamics simulation for system size from $N = 8, 10, 12$ and circuit depth $D = N/2 + 1$ which is sufficient to capture the exact imaginary-time dynamics. The initial state is determined by randomly flipping (applying X gates) on half of the qubits at the beginning of the circuit. The results are consistent with the critical exponent $\theta = 0.373$ for 1D TFIM from the data collapse according to Eq. (5) as shown in Fig. 6.

APPENDIX G: FINITE SIZE SCALING AND DATA COLLAPSE ANALYSIS

The scaling analysis procedure is similar to the approach presented in Appendix A in [69]. We use the fit on data in Fig. 3 in the main text as an example to showcase the workflow, the fit on data in other figures is similar.

For a set of estimated exponents of β/ν and α, one can define a cost function $R(\beta/\nu, \alpha)$ and try to minimize the cost

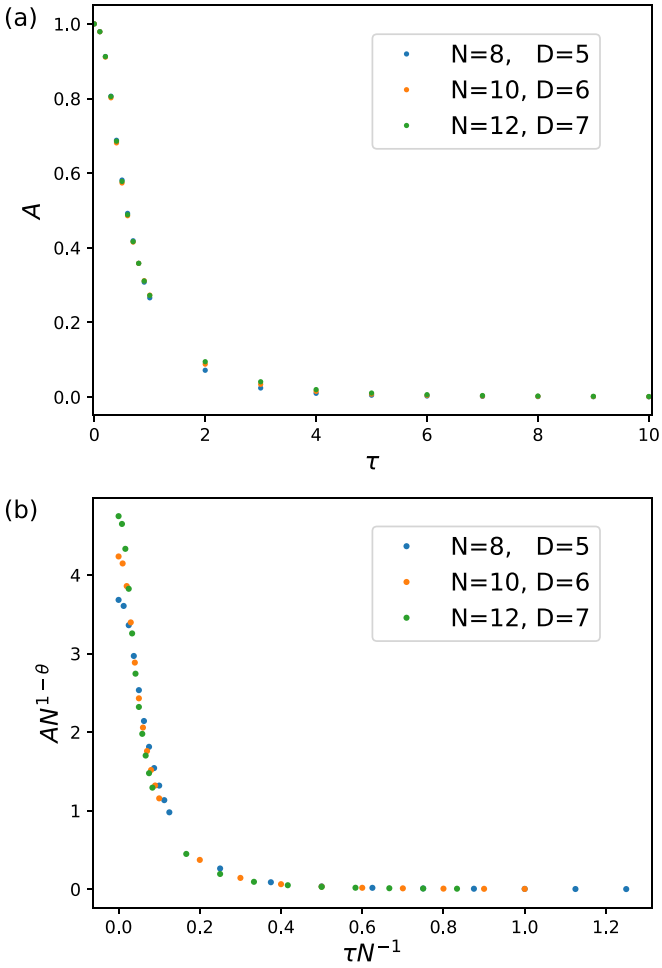

FIG. 6. Imaginary-time correlator A (a) unscaled and (b) finite-size scaled. The imaginary-time dynamics related critical exponent $\theta \approx 0.373$.

by searching optimal values for β/ν and α. First, we rescale the data in each group (D_i, M_i) (fixed τ/N, different size N) as $x_i = DN^{-\alpha}$ and $y_i = MN^{\beta/\nu}$, leading to a family of curves $y_N(x)$, one curve for each system size N. The cost function R is defined as the sum of the mean-squared deviations of each curve from their mean, summed over all unique points x_i in the data set. In other words,

$$R = \sum_{i,N} [y_N(x_i) - \bar{y}(x_i)]^2,$$

where $y_N(x_i)$ indicates the value of y_N at the point x_i. If this value is not specified explicitly in the data, it can be estimated by linear interpolation. Note that $\bar{y}(x)$ is the mean value of $y_N(x)$ over different system sizes N. For multiple variable scaling fit such as Fig. 3 in the main text, we also need to sum the cost function for each group of different τ/N. The physical meaning is that we expect to identify the suitable exponents such that data points of the same τ/N lie on the same curve while points of different τ/N belong to different curves.

Given the numerical data, we can locate the best guess on critical exponents by extensive grid search since there are only two variables. The grid search result is similar to Fig. 3(c) in the main text and we can extract the optimal estimation for the exponents as well as the error bar by specifying some threshold on the cost function.

Specifically, for the data collapse of Fig. 2 in the main text, we use imaginary time evolution data from $N = 8,\ 10,\ 12$ and circuit depth $D = N/2 + 1$ at $0.2 \leqslant \tau \leqslant 10$. We assume a prior of $z = 1$ and fit the single exponent β/ν by grid search.

For the data collapse of Fig. 3, we also assume $z = 1$ as a prior, and try to identify the best β/ν and finite depth exponent α at the same time. We use the numerical results from seven curves $\tau/N = 0.1,\ 0.2,\ 0.3,\ 0.4,\ 0.5,\ 0.6,\ 0.7$, with system size $N = 8,\ 10,\ 12$ and circuit depth $2 \leqslant D \leqslant 8$ to fit the scaling behavior.

APPENDIX H: FINITE-DEPTH SCALING EXTRACTED FROM GROUND STATE SIMULATION

To disentangle different scaling factors (imaginary time τ and circuit depth D) and better understand them, we directly utilize variational ground state simulation to extract the finite-depth critical exponent. The ground state can be taken as the limit of infinite time $\tau \to \infty$ in the context of imaginary time evolution and we expect the scaling form as

$$M^2(L, D) = N^{-2\beta/\nu} f_M(N^{-\alpha} D). \tag{H1}$$

To solve the ground state problem, the variational quantum eigensolver (VQE) algorithm is utilized. In VQE, we directly minimize $E(\theta) = \langle 0|U(\vec{\theta})^\dagger H U(\vec{\theta})|0\rangle$ by tuning the parameters θ based on gradient descent, i.e., $\theta = \theta - \epsilon \frac{\partial E(\theta)}{\partial \theta}$, where ϵ is the learning rate. These circuit parameter gradients can be obtained via the parameter shift scheme in experiments and be more efficiently simulated classically via automatic differentiation integrated with TENSORCIRCUIT.

We use the same Hamiltonian model and circuit ansatz as given in the main text to run the VQE. For each system size N and circuit depth D, we run independent optimization over 64 different random initialization parameters sampled from Gaussian distribution with center 0 and standard deviation 0.1. The optimal final results of these 64 trials are reported to avoid local minimum issues. We run the gradient descent 10000 steps to ensure the convergence with the Adam optimizer and an exponential decay learning rate schedule. The hyperparameter of the optimizer is tuned for better convergence speed and accuracy. The order parameter M^2 of the converged state with different sizes N and depth D are shown in Fig. 7(a). And we can do a finite-size finite-depth scaling on the data to extract critical exponent for depth α according to Eq. (H1), see Fig. 7(b). The exponent is estimated as $\alpha = 1.28 \pm 0.06$. This value is very similar to the exponent reported in [49] where 1.21, 1.07 are estimated for translational invariant infinite size circuit on 1D TFIM model for entanglement entropy and order parameter, respectively. To demonstrate such finite depth exponent is universal, we apply VQE with very different circuit ansatz on the same Hamiltonian, and the result on α is consistent as explained below. The α estimated from VQE here is also very close to the result in the main text extracted from the dynamics simulation.

To demonstrate the universality of the finite-depth exponent α, we also carry out VQE with different circuit ansatz.

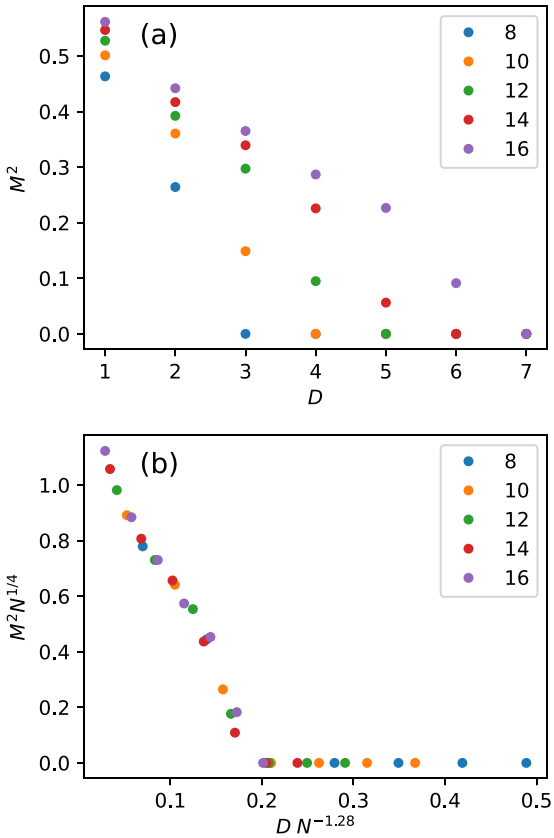

FIG. 7. (a) M^2 of converged quantum state after VQE optimization on quantum computers of different sizes N and depths D. (b) Data collapse for the converged state on quantum computers of different sizes and depths. We estimate the critical exponent for the depth scaling as $\alpha = 1.28 \pm 0.06$.

The alternative ansatz has the brickwall two-qubit layout and less density of single-qubit gates and hence less expressive power with the same depth D. Specifically, the alternative circuit structure (see Fig. 8) is composed of D blocks of Rx gates and two-qubit gates $e^{i\theta Z_i Z_{i+1}}$ are placed in an even-odd brickwall fashion instead of the ladder layout in the main text.

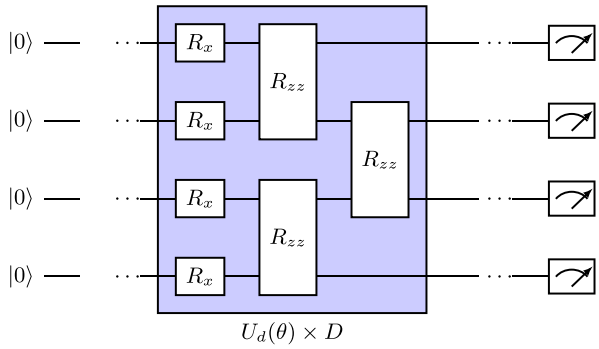

FIG. 8. The alternative variational circuit ansatz for VQE to demonstrate the universal finite-depth scaling. Each block is composed of only one layer of Rx gates and one layer of Rzz gates in the brickwall layout.

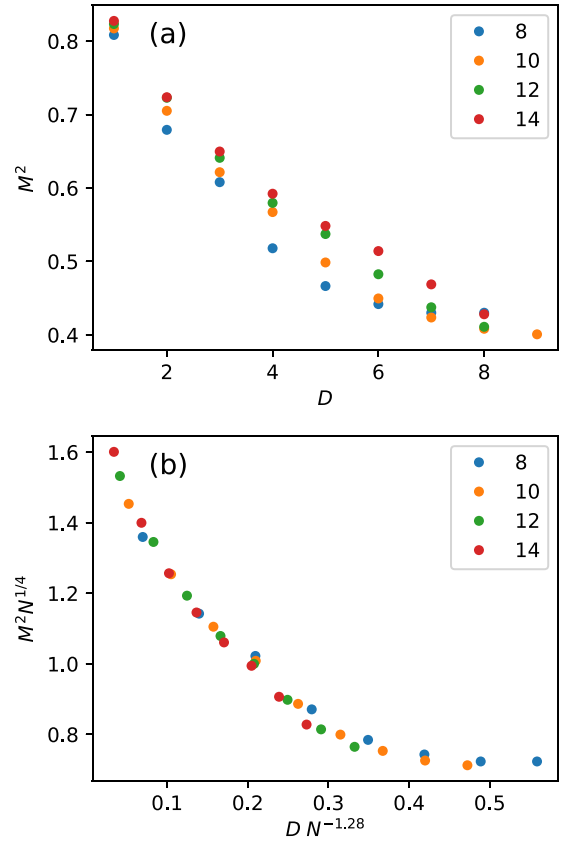

FIG. 9. (a) M^2 of converged quantum state after VQE optimization on quantum computers of different sizes N and depth D with alternative ansatz. (b) Data collapse for the converged state on quantum computers of different sizes and depths. The critical exponent for the depth scaling is $\alpha = 1.28 \pm 0.07$, consistent with the circuit ansatz in the main text.

Each block U_d can be expressed as

$$U_d(\theta_d) = \prod_{i\in\text{odd}}^{N} e^{-i\theta_{id2} Z_i Z_{i+1}} \prod_{i\in\text{even}}^{N} e^{-i\theta_{id2} Z_i Z_{i+1}} \prod_{i=1}^{N} e^{-i\theta_{id1} X_i}. \tag{H2}$$

The extracted depth critical exponent α in this case is consistent with the former ansatz, implying a universal finite depth exponent for VQE of TFIM Hamiltonian. The result is summarized as Fig. 9.

APPENDIX I: SCALING ANALYSIS WITH DATA FROM EVEN EARLIER TIMES AND SHALLOWER CIRCUITS

For the scaling analysis on data from Fig. 3, we note that even if we only include data with short time and small depth, we can still capture the qualitatively correct scaling behavior. For example, if we only include data with $\tau/N = 0.1,\ 0.2,\ 0.3,\ 0.4$ and circuit depth $2 \leqslant D \leqslant 5$, we can still obtain similar critical exponent estimation as shown in Fig. 10. The estimated result deviates from the exact value a little. However, considering how shallow the circuit is and how short time we are using, the relatively reasonable estimation we obtain demonstrates the key point of this work:

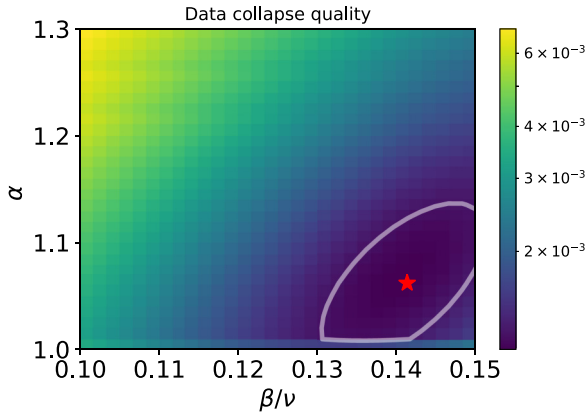

FIG. 10. Data collapse quality grid search with variational imaginary time dynamics data of size $N = 8,\ 10,\ 12$, circuit depth $D = 2,\ 3,\ 4,\ 5$, and time $\tau/N = 0.1,\ 0.2,\ 0.3,\ 0.4$. The optimal exponents estimate is $\alpha = 1.06 \pm 0.03$ and $\beta/\nu = 0.14 \pm 0.05$. The grey contour indicates the boundary where the cost function is 10% worse than the optimal estimate.

we can access the universal critical properties via finite-size, short-time and finite-depth scaling. Via finite-size scaling, we can probe the thermodynamic behavior via small size system; via short-time scaling, we can probe the ground state behavior at the early imaginary time stage; and via finite-depth scaling, we can probe the exact imaginary-time dynamics with shallower circuits and large approximation error. Putting these scaling forms together, we can investigate universal properties of interesting quantum systems on quantum computers in a scalable and efficient way.

APPENDIX J: EXPERIMENTAL QUANTUM HARDWARE

All experiments were performed on the 20-qubit quantum device. The same series of quantum processors have been reported before in other experimental works [55,70]. The topology of the device is a 10×2 grid, see Fig. 11. In the experiment, we only utilize the second row of the qubits (qubit 12-19 for 8-qubit experiment, qubit 13-19 for 7 qubit-experiment, and qubit 14-19 for 6 qubit-experiment). Typical mean error rates of qubit 12-19 are 1.6×10^{-2} for two-qubit gates, 0.14×10^{-2} for single-qubit gates and 7×10^{-2} for readout errors. Mean T_1 and T_2 time for qubit 12-19 are 24 and 5 μs, respectively.

APPENDIX K: COMPARISON OF EXPERIMENT RESULTS BEFORE AND AFTER DATA COLLAPSE

The mitigated results from the quantum hardware experiment are presented before and after the correct data collapse (axis finite-size rescaling). See Fig. 12.

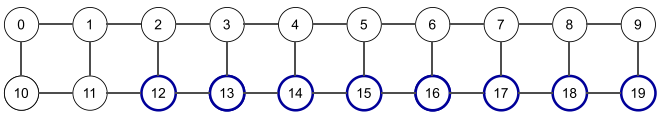

FIG. 11. The qubit layout and coupling map for the 20-qubit device. The qubits with blue circles are used in the experiment of this work.

APPENDIX L: QUANTUM ERROR MITIGATION SCHEME

To evaluate M, the sum of expectation of local Pauli Z operators, from quantum computers, we utilize two methods to mitigate the errors. We firstly apply scalable readout error mitigation on observable expectation level natively assuming local tensor product structure of the readout error [56]. This approach works well in practice since the readout error on the device is well approximated by local structures with very little readout error correlation across qubits. We label the experimental results with only readout error mitigation *raw*. To apply such readout error mitigation on expectations, we use the built-in readout error mitigator for observable expectations in TENSORCIRCUIT [54]. The exact formula for the readout error mitigation in this case can be derived analytically. Suppose the target observable is Pauli Z operator on qubit i as $\langle Z_i \rangle$ and the readout error rates for 0 to 1 and 1 to 0 are ϵ_i and η_i on qubit i, respectively. Note that these local readout error rates can be calibrated by simply running two benchmark circuits. For each readout result of 0 state on qubit i, we count the contribution to $\langle Z_i \rangle$ as $\frac{1+\epsilon_i-\eta_i}{1-\epsilon_i-\eta_i}$ instead of simply $+1$. Similarly, for each readout result of 1 state on qubit i, we count the contribution to $\langle Z_i \rangle$ as $-\frac{1-\epsilon_i+\eta_i}{1-\epsilon_i-\eta_i}$ instead of -1. Such a formula is the direct consequence of Eq. (6) in Ref. [56].

The accuracy for *raw* results with only readout error mitigation is not sufficient to observe universal imaginary-time dynamics due to the quantum noise on the quantum chip. We further apply Clifford data regression (CDR) approach [10,11] to mitigate quantum errors and obtain reliable expectation estimation for order parameter M. The basic idea behind CDR is to firstly build several similar near Clifford circuits close to the target circuit to be evaluated. We then run each near Clifford circuit on both quantum hardware and the classical simulator to obtain two sets of results M_{noisy} and M_{ideal} for each near Clifford circuit instance. Via the data of M_{noisy} and M_{ideal}, we can fit a linear regression relation by the least square method, i.e., $M_{\text{ideal}} = aM_{\text{noisy}} + b$ where a, b are learning parameters. Finally, by running our target circuit on the quantum hardware with the results as M_{noisy}, we can recover M_{ideal} for the target circuit via the linear regression relation. In our experiment, we build several groups of circuit samples with different ratios of non-Clifford gates, and train them together to obtain the linear relation. We call this specific method extended CDR. We believe training on data with multiple non-Clifford ratios can make CDR results more robust and reliable. For each group i, we build n_i circuits by uniformly replacing approximately $1 - r_i$ ratio of non-Clifford single-qubit gates to the closest Clifford gate (in terms of Rz rotation angles). For small time scale $\tau < 1$, the prediction inaccuracy on the hardware is relatively small, so we use $n_1 = 5$, $r_1 = 0.6$, $n_2 = 5$, $r_2 = 0.7$, $n_3 = 5$, $r_3 = 0.8$, and $n_4 = 5$, $r_4 = 0.9$, four groups and 20 circuits in total to learn the linear relation between the noisy prediction of M on the chip and the ideal expectation of M simulated classically. For larger τ, the true value of M_{ideal} is smaller and the experiment accuracy becomes worse, so we use $n_1 = 5$, $r_1 = 0.8$, $n_2 = 5$, $r_2 = 0.9$, $n_3 = 5$, $r_3 = 0.95$ three groups and 15 circuits to learn the linear prior. The results obtained using this CDR pipeline are labeled as *mit*. To apply CDR error mitigation technique, we use the CDR method from Mitiq [71] with

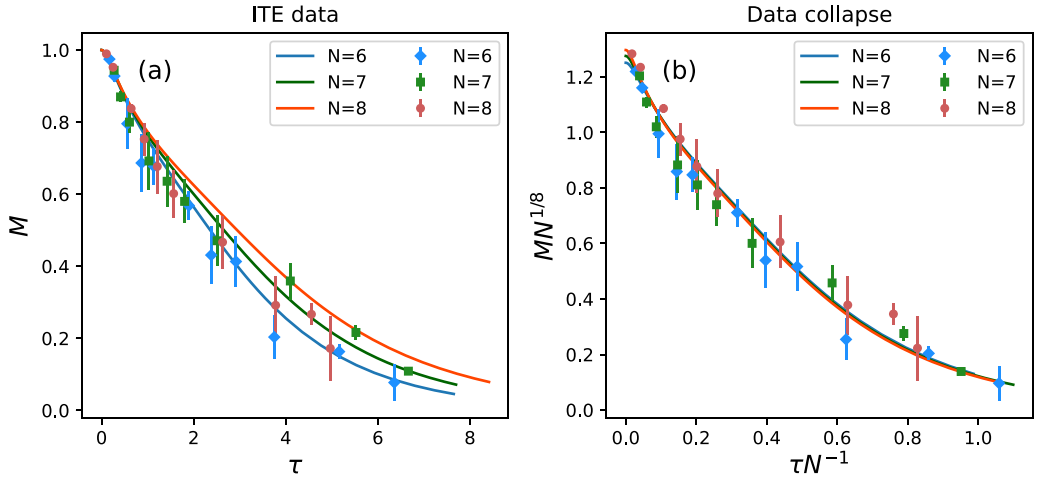

FIG. 12. (a) Experimental results from quantum computers via error mitigation. (b) The data collapse. All data points are expected to fall into the same curve in the ideal case.

further customization on multiple non-Clifford ratio support and TENSORCIRCUIT compatibility. It is worth noting that the specific CDR approach we adopt here has a very high ratio of r_i on average indicating scalability issues. A high ratio of non-Clifford gate can lead to a circuit data with similar M as the original circuit which greatly improves the accuracy for *mit* results in our experiment. In other words, a very low ratio of non-Clifford gates such as $r = 0.1$ is not sufficient to give stable and accurate mitigated experimental results now due to the relatively large quantum noise, especially cross-talk error present on the current generation quantum chip. Such high ratios cannot be maintained for larger system sizes when stabilizer circuit simulation formalism is required where the simulation complexity is exponential with the number of non-Clifford T gates. Our perspective is, that with further development of the quantum hardware, the experiment will be impacted by less quantum noise and the corresponding non-Clifford ratio r in CDR can go down to the classical simulatable regime even with larger system size in the future.

[1] J. Preskill, Quantum computing in the NISQ era and beyond, Quantum **2**, 79 (2018).

[2] F. Arute, K. Arya, R. Babbush, D. Bacon, J. C. Bardin, R. Barends, R. Biswas, S. Boixo, F. G. S. L. Brandao, D. A. Buell, B. Burkett, Y. Chen, Z. Chen, B. Chiaro, R. Collins, W. Courtney, A. Dunsworth, E. Farhi, B. Foxen, A. Fowler *et al.*, Quantum supremacy using a programmable superconducting processor, Nature (London) **574**, 505 (2019).

[3] Y. Kim, A. Eddins, S. Anand, K. X. Wei, E. van den Berg, S. Rosenblatt, H. Nayfeh, Y. Wu, M. Zaletel, K. Temme, and A. Kandala, Evidence for the utility of quantum computing before fault tolerance, Nature (London) **618**, 500 (2023).

[4] K. Bharti, A. Cervera-Lierta, T. H. Kyaw, T. Haug, S. Alperin-Lea, A. Anand, M. Degroote, H. Heimonen, J. S. Kottmann, T. Menke, W.-K. Mok, S. Sim, L.-C. Kwek, and A. Aspuru-Guzik, Noisy intermediate-scale quantum algorithms, Rev. Mod. Phys. **94**, 015004 (2022).

[5] M. Cerezo, A. Arrasmith, R. Babbush, S. C. Benjamin, S. Endo, K. Fujii, J. R. McClean, K. Mitarai, X. Yuan, L. Cincio, and P. J. Coles, Variational quantum algorithms, Nat. Rev. Phys. **3**, 625 (2021).

[6] S. Endo, Z. Cai, S. C. Benjamin, and X. Yuan, Hybrid quantum-classical algorithms and quantum error mitigation, J. Phys. Soc. Jpn. **90**, 032001 (2021).

[7] J. Tilly, H. Chen, S. Cao, D. Picozzi, K. Setia, Y. Li, E. Grant, L. Wossnig, I. Rungger, G. H. Booth, and J. Tennyson, The variational quantum eigensolver: A review of methods and best practices, Phys. Rep. **986**, 1 (2022).

[8] Z. Cai, R. Babbush, S. C. Benjamin, S. Endo, W. J. Huggins, Y. Li, J. R. McClean, and T. E. O'Brien, Quantum error mitigation, Rev. Mod. Phys. **95**, 045005 (2023).

[9] K. Temme, S. Bravyi, and J. M. Gambetta, Error mitigation for short-depth quantum circuits, Phys. Rev. Lett. **119**, 180509 (2017).

[10] P. Czarnik, A. Arrasmith, P. J. Coles, and L. Cincio, Error mitigation with Clifford quantum-circuit data, Quantum **5**, 592 (2021).

[11] A. Lowe, M. H. Gordon, P. Czarnik, A. Arrasmith, P. J. Coles, and L. Cincio, Unified approach to data-driven quantum error mitigation, Phys. Rev. Res. **3**, 033098 (2021).

[12] Y. Kim, C. J. Wood, T. J. Yoder, S. T. Merkel, J. M. Gambetta, K. Temme, and A. Kandala, Scalable error mitigation for noisy quantum circuits produces competitive expectation values, Nat. Phys. **19**, 752 (2023).

[13] A. Strikis, D. Qin, Y. Chen, S. C. Benjamin, and Y. Li, Learning-based quantum error mitigation, PRX Quantum **2**, 040330 (2021).

[14] S.-X. Zhang, Z.-Q. Wan, C.-Y. Hsieh, H. Yao, and S. Zhang, Variational quantum-neural hybrid error mitigation, Adv. Quantum Technol. **6**, 202300147 (2023).

[15] S. Sachdev, *Quantum Phase Transitions* (Cambridge University Press, Cambridge, 2011).

[16] A. Peruzzo, J. McClean, P. Shadbolt, M.-H. Yung, X.-Q. Zhou, P. J. Love, A. Aspuru-Guzik, and J. L. O'Brien, A variational eigenvalue solver on a photonic quantum processor, Nat. Commun. **5**, 4213 (2014).

[17] J.-G. Liu, Y.-H. Zhang, Y. Wan, and L. Wang, Variational quantum eigensolver with fewer qubits, Phys. Rev. Res. **1**, 023025 (2019).

[18] S. McArdle, S. Endo, A. Aspuru-Guzik, S. C. Benjamin, and X. Yuan, Quantum computational chemistry, Rev. Mod. Phys. **92**, 015003 (2020).

[19] S.-X. Zhang, Z.-Q. Wan, C.-K. Lee, C.-Y. Hsieh, S. Zhang, and H. Yao, Variational quantum-neural hybrid eigensolver, Phys. Rev. Lett. **128**, 120502 (2022).

[20] S. Liu, S.-X. Zhang, C.-Y. Hsieh, S. Zhang, and H. Yao, Probing many-body localization by excited-state variational quantum eigensolver, Phys. Rev. B **107**, 024204 (2023).

[21] J. Miao, C.-Y. Hsieh, and S.-X. Zhang, Neural-network-encoded variational quantum algorithms, Phys. Rev. Appl. **21**, 014053 (2024).

[22] S. Liu, S.-X. Zhang, S.-K. Jian, and H. Yao, Training variational quantum algorithms with random gate activation, Phys. Rev. Res. **5**, L032040 (2023).

[23] Y. Li and S. C. Benjamin, Efficient variational quantum simulator incorporating active error minimization, Phys. Rev. X **7**, 021050 (2017).

[24] S. McArdle, T. Jones, S. Endo, Y. Li, S. C. Benjamin, and X. Yuan, Variational ansatz-based quantum simulation of imaginary time evolution, npj Quantum Inf. **5**, 75 (2019).

[25] X. Yuan, S. Endo, Q. Zhao, Y. Li, and S. C. Benjamin, Theory of variational quantum simulation, Quantum **3**, 191 (2019).

[26] C. K. Lee, S.-X. Zhang, C.-Y. Hsieh, S. Zhang, and L. Shi, Variational quantum simulations of finite-temperature dynamical properties via thermofield dynamics, arXiv:2206.05517.

[27] Y.-M. Ding, Y.-C. Wang, S.-X. Zhang, and Z. Yan, Exploring the topological sector optimization on quantum computers, arXiv:2310.04291.

[28] T. W. B. Kibble, Topology of cosmic domains and strings, J. Phys. A: Math. Gen. **9**, 1387 (1976).

[29] W. H. Zurek, Cosmological experiments in superfluid helium? Nature (London) **317**, 505 (1985).

[30] J. Dziarmaga, Dynamics of a quantum phase transition and relaxation to a steady state, Adv. Phys. **59**, 1063 (2010).

[31] A. Polkovnikov, K. Sengupta, A. Silva, and M. Vengalattore, Colloquium : Nonequilibrium dynamics of closed interacting quantum systems, Rev. Mod. Phys. **83**, 863 (2011).

[32] Y. Huang, S. Yin, B. Feng, and F. Zhong, Kibble-Zurek mechanism and finite-time scaling, Phys. Rev. B **90**, 134108 (2014).

[33] A. D. King, J. Raymond, T. Lanting, R. Harris, A. Zucca, F. Altomare, A. J. Berkley, K. Boothby, S. Ejtemaee, C. Enderud, E. Hoskinson, S. Huang, E. Ladizinsky, A. J. R. MacDonald, G. Marsden, R. Molavi, T. Oh, G. Poulin-Lamarre, M. Reis, C. Rich *et al.*, Quantum critical dynamics in a 5,000-qubit programmable spin glass, Nature (London) **617**, 61 (2023).

[34] A. Keesling, A. Omran, H. Levine, H. Bernien, H. Pichler, S. Choi, R. Samajdar, S. Schwartz, P. Silvi, S. Sachdev, P. Zoller, M. Endres, M. Greiner, V. Vuletić, and M. D. Lukin, Quantum Kibble–Zurek mechanism and critical dynamics on a programmable Rydberg simulator, Nature (London) **568**, 207 (2019).

[35] L. W. Clark, L. Feng, and C. Chin, Universal space-time scaling symmetry in the dynamics of bosons across a quantum phase transition, Science **354**, 606 (2016).

[36] B. Ko, J. W. Park, and Y. Shin, Kibble–Zurek universality in a strongly interacting Fermi superfluid, Nat. Phys. **15**, 1227 (2019).

[37] S. Ulm, J. Roßnagel, G. Jacob, C. Degünther, S. T. Dawkins, U. G. Poschinger, R. Nigmatullin, A. Retzker, M. B. Plenio, F. Schmidt-Kaler, and K. Singer, Observation of the Kibble–Zurek scaling law for defect formation in ion crystals, Nat. Commun. **4**, 2290 (2013).

[38] S. Yin, P. Mai, and F. Zhong, Universal short-time quantum critical dynamics in imaginary time, Phys. Rev. B **89**, 144115 (2014).

[39] S. Zhang, S. Yin, and F. Zhong, Generalized dynamic scaling for quantum critical relaxation in imaginary time, Phys. Rev. E **90**, 042104 (2014).

[40] Y.-R. Shu, S. Yin, and D.-X. Yao, Universal short-time quantum critical dynamics of finite-size systems, Phys. Rev. B **96**, 094304 (2017).

[41] Y.-K. Yu, Z. Zeng, Y.-R. Shu, Z.-X. Li, and S. Yin, Nonequilibrium dynamics in Dirac quantum criticality, arXiv:2310.10601.

[42] J.-Q. Cai, Y.-R. Shu, X.-Q. Rao, and S. Yin, Imaginary-time relaxation quantum critical dynamics in two-dimensional dimerized Heisenberg model, arXiv:2403.09084.

[43] B. Zheng, Generalized dynamic scaling for critical relaxations, Phys. Rev. Lett. **77**, 679 (1996).

[44] H. K. Janssen, B. Schaub, and B. Schmittmann, New universal short-time scaling behaviour of critical relaxation processes, Z. Phys. B **73**, 539 (1989).

[45] Z. B. Li, L. Schülke, and B. Zheng, Dynamic monte carlo measurement of critical exponents, Phys. Rev. Lett. **74**, 3396 (1995).

[46] Z. Li, L. Schülke, and B. Zheng, Finite-size scaling and critical exponents in critical relaxation, Phys. Rev. E **53**, 2940 (1996).

[47] B. Zheng, Monte Carlo simulations of short-time critical dynamics, Int. J. Mod. Phys. B **12**, 1419 (1998).

[48] C. Bravo-Prieto, J. Lumbreras-Zarapico, L. Tagliacozzo, and J. I. Latorre, Scaling of variational quantum circuit depth for condensed matter systems, Quantum **4**, 272 (2020).

[49] B. Jobst, A. Smith, and F. Pollmann, Finite-depth scaling of infinite quantum circuits for quantum critical points, Phys. Rev. Res. **4**, 033118 (2022).

[50] M. Motta, C. Sun, A. T. K. Tan, M. J. O'Rourke, E. Ye, A. J. Minnich, F. G. S. L. Brandão, and G. K.-l. L. Chan, Determining eigenstates and thermal states on a quantum computer using quantum imaginary time evolution, Nat. Phys. **16**, 205 (2020).

[51] M. Benedetti, M. Fiorentini, and M. Lubasch, Hardware-efficient variational quantum algorithms for time evolution, Phys. Rev. Res. **3**, 033083 (2021).

[52] S. Barison, F. Vicentini, and G. Carleo, An efficient quantum algorithm for the time evolution of parameterized circuits, Quantum **5**, 512 (2021).

[53] R. Wiersema, C. Zhou, Y. de Sereville, J. F. Carrasquilla, Y. B. Kim, and H. Yuen, Exploring entanglement and optimization within the hamiltonian variational ansatz, PRX Quantum **1**, 020319 (2020).

[54] S.-X. Zhang, J. Allcock, Z.-Q. Wan, S. Liu, J. Sun, H. Yu, X.-H. Yang, J. Qiu, Z. Ye, Y.-Q. Chen, C.-K. Lee, Y.-C. Zheng, S.-K. Jian, H. Yao, C.-Y. Hsieh, and S. Zhang, TENSORCIRCUIT:

a quantum software framework for the NISQ era, Quantum **7**, 912 (2023).

[55] L. Cheng, Y.-Q. Chen, S.-X. Zhang, and S. Zhang, Error-mitigated quantum approximate optimization via learning-based adaptive optimization, Commun. Phys. **7**, 83 (2024).

[56] S. Bravyi, S. Sheldon, A. Kandala, D. C. Mckay, and J. M. Gambetta, Mitigating measurement errors in multi-qubit experiments, Phys. Rev. A **103**, 042605 (2021).

[57] G. Vidal, Class of quantum many-body states that can be efficiently simulated, Phys. Rev. Lett. **101**, 110501 (2008).

[58] G. Evenbly and G. Vidal, Algorithms for entanglement renormalization, Phys. Rev. B **79**, 144108 (2009).

[59] I. H. Kim and B. Swingle, Robust entanglement renormalization on a noisy quantum computer, arXiv:1711.07500.

[60] T. J. Sewell, N. Bao, and S. P. Jordan, Variational quantum simulation of the critical Ising model with symmetry averaging, Phys. Rev. A **107**, 042620 (2023).

[61] Y.-X. Yao, N. Gomes, F. Zhang, C.-Z. Wang, K.-M. Ho, T. Iadecola, and P. P. Orth, Adaptive variational quantum dynamics simulations, PRX Quantum **2**, 030307 (2021).

[62] S.-X. Zhang, C.-Y. Hsieh, S. Zhang, and H. Yao, Differentiable quantum architecture search, Quantum Sci. Technol. **7**, 045023 (2022).

[63] S.-X. Zhang, C.-Y. Hsieh, S. Zhang, and H. Yao, Neural predictor based quantum architecture search, Mach. Learn.: Sci. Technol. **2**, 045027 (2021).

[64] Y. Du, T. Huang, S. You, M.-H. Hsieh, and D. Tao, Quantum circuit architecture search for variational quantum algorithms, npj Quantum Inf. **8**, 62 (2022).

[65] Z. Lu, P.-X. Shen, and D.-L. Deng, Markovian quantum neuroevolution for machine learning, Phys. Rev. Appl. **16**, 044039 (2021).

[66] A. McLachlan, A variational solution of the time-dependent Schrodinger equation, Mol. Phys. **8**, 39 (1964).

[67] T. Liu, J.-G. Liu, and H. Fan, Probabilistic nonunitary gate in imaginary time evolution, Quantum Info. Proc. **20**, 204 (2021).

[68] P. Virtanen, R. Gommers, T. E. Oliphant, M. Haberland, T. Reddy, D. Cournapeau, E. Burovski, P. Peterson, W. Weckesser, J. Bright, S. J. van der Walt, M. Brett, J. Wilson, K. J. Millman, N. Mayorov, A. R. J. Nelson, E. Jones, R. Kern, E. Larson, C. J. Carey *et al.*, SciPy 1.0: fundamental algorithms for scientific computing in Python, Nature Methods **17**, 261 (2020).

[69] B. Skinner, J. Ruhman, and A. Nahum, Measurement-induced phase transitions in the dynamics of entanglement, Phys. Rev. X **9**, 031009 (2019).

[70] W. Li, J. Ren, S. Huai, T. Cai, Z. Shuai, and S. Zhang, Efficient quantum simulation of electron-phonon systems by variational basis state encoder, Phys. Rev. Res. **5**, 023046 (2023).

[71] R. LaRose, A. Mari, S. Kaiser, P. J. Karalekas, A. A. Alves, P. Czarnik, M. El Mandouh, M. H. Gordon, Y. Hindy, A. Robertson, P. Thakre, M. Wahl, D. Samuel, R. Mistri, M. Tremblay, N. Gardner, N. T. Stemen, N. Shammah, and W. J. Zeng, MITIQ: A software package for error mitigation on noisy quantum computers, Quantum **6**, 774 (2022).